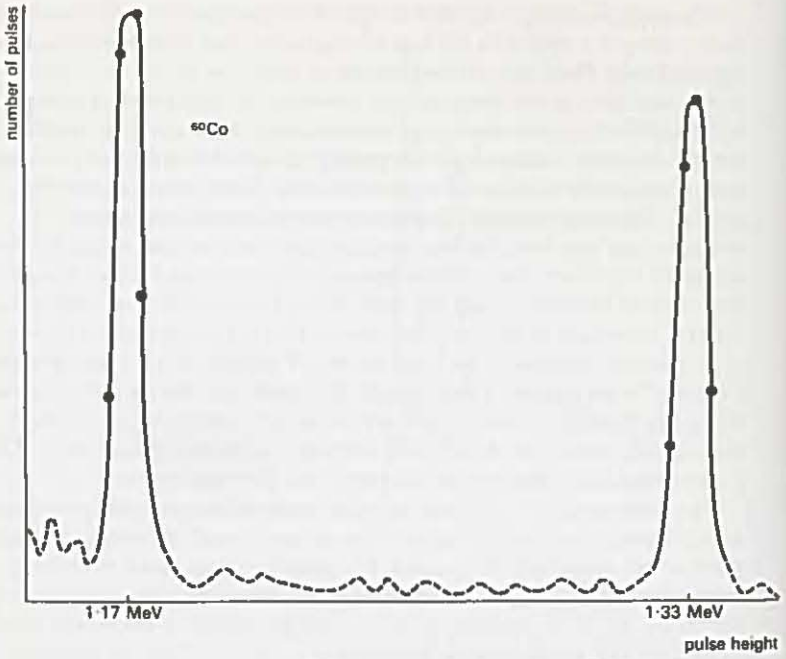

Figure 74 Energy spectrum of ^{60}Co measured with a 40 cm^3 Li-Ge detector, showing the total energy peaks for the 1·17 MeV and 1·33 MeV γ-ray lines

10.12 The measurement of lifetimes of excited states

The measurement of the lifetimes of excited states, when the transitions are of high multipole order and therefore fall into the category of isomeric transitions, as discussed in section 6.10, represents the same problem as the measurement of the lifetimes of α- and β-emitters. The numbers of γ-rays N_γ emitted in equal intervals of time, shorter than or comparable with the half-life, are measured. A plot of $\ln N_\gamma$ against t then results in a straight line of negative slope λ, where λ is the total transition probability. Electronic timing of the intervals, with the counts being delivered to a set of scaling circuits and mechanical counters, allows this direct technique to be extended down to half-lives in the microsecond (10^{-6} s) region. Using only the front edges of pulses from scintillation detectors, or using fast pulses from solid-state detectors in conjunction with delay lines and fast coincidence circuits, half-lives down to 10^{-10} s may be measured by an extension of the direct technique. There is still a gap of many orders of magnitude between this range of lifetimes and the half-lives anticipated for lower multipole order transitions.

In certain circumstances a further range of half-lives extending down to picoseconds (10^{-12} s) can now be explored using the Doppler shift of γ-ray energy

which occurs when the emitting nucleus is recoiling. This extension has proved important, as we shall see later, in the information that it has given concerning the transition probabilities of E2 transitions.

We begin discussion of this method, referred to as the *Doppler shift attenuation method* (DSAM) by making the unrealistic assumption that we are dealing with a set of nuclei all produced in excited states by bombardment with heavy projectiles, and all recoiling into vacuum in the same direction with identical velocities. Suppose a stop is arranged as shown in Figure 75, and make the further

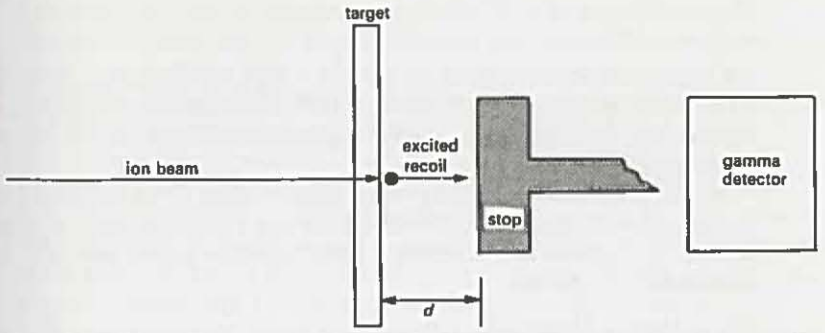

Figure 75 Schematic representation of Doppler shift attenuation measurement of lifetime of excited state

assumption that the recoils, which will be highly charged particles, are brought to rest instantaneously when they enter the stop. If the mean life τ of the excited state is short compared to the time of transit of the recoils from the target to the stop, d/v, then most of the nuclei will de-excite in flight before hitting the stop. The wavelength (and hence frequency and energy) of the radiation will be modified by the velocity of the source according to the well-known Doppler effect. If $v \ll c$, the photons emitted by the recoiling nuclei at 0° to their direction of travel will have an energy

$$E = E_0\left[1 + \frac{v}{c}\right],$$

where E_0 is the transition energy. The recoils which survive the transit without de-exciting will be stationary in the stop when emission takes place. They will emit photons of the full energy E_0.

The analysis developed in Chapter 2 for radioactive decay can of course be applied directly to the de-excitation of the excited nuclei. The probability that a nucleus will *not* decay in a time t, measured from its instant of emission from the target, is given by $\exp(-\lambda t)$. Thus, the time of flight from target to stop being d/v, the ratio of nuclei de-exciting in flight will be given by

$$\frac{e^{-\lambda d/v}}{1 - e^{-\lambda d/v}}.$$

$$-\frac{dE}{dx}=-M\frac{dv}{dt}=M\frac{v}{\alpha},$$

and write $\dfrac{dv}{dt}=-\dfrac{v}{\alpha}$.

Thus $v(t)=v_0e^{-t/\alpha}$

We can now write

$$F(\tau)=\frac{1}{v_0\tau}\int_0^{\infty}v_0\,e^{-t(1/\alpha+1/\tau)}\,dt=\frac{\alpha}{\alpha+\tau}=\frac{\lambda\alpha}{1+\lambda\alpha}. \qquad 10.6$$

A measurement of the mean Doppler shift, and its comparison with the maximum Doppler shift, then gives the attenuation function $F(\tau)$, from which τ can be found using equation **10.6**. It is clear from the form of this equation that the method will be most sensitive when $\lambda\alpha \simeq 1$. The observed values of α for solid materials lie in the range 0·1–1 ps and hence the DSAM technique is most suited for measurements of half-lives in the neighbourhood of a picosecond.

10.13 The measurements of level widths

We noted in section 10.7 that the product of the mean life of the level and its width equalled $\hbar$. Thus the measurement of the level width provides essentially the same information as the measurement of the mean life. However level-width measurements can sometimes be achieved for states where the mean life is too short to be measured by the methods discussed in section 10.12.

We begin by considering quantitatively the nature of the problem of measuring the level width in a particular case. For a nucleus with A approximately 125 and a level at say 200 keV, the 'single-particle' estimates of width quoted in section 10.7 become

$$\text{E1} = 1{\cdot}38 \times 10^{-2}\ \text{eV},$$
$$\text{E2} = 0{\cdot}98 \times 10^{-8}\ \text{eV},$$
$$\text{E3} = 4{\cdot}6 \times 10^{-15}\ \text{eV},$$
$$\text{M1} = 1{\cdot}68 \times 10^{-4}\ \text{eV},$$
$$\text{M2} = 1{\cdot}2 \times 10^{-10}\ \text{eV},$$
$$\text{M3} = 5{\cdot}44 \times 10^{-17}\ \text{eV}.$$

These estimates depend of course on the nuclear model from which the wave functions have been taken to calculate the matrix element, and should be considered only as a guide to likely orders of magnitudes of level widths. It is clear that it is not practical to explore the resonances by a direct method, either for example by measuring with sufficient resolution the emitted photon spectrum or by measuring the absorption by the nucleus of a beam of photons of sufficiently

limited energy spread. The resolution of available γ-ray spectrometers, as was seen in section 10.12, is many orders of magnitude too low. Photon beams in the energy range of interest are not available with anything approaching the degree of energy homogeneity that would be necessary for a direct absorption experiment. It might seem that the photon emitted from a transition to the ground state would be strongly absorbed by an unexcited nucleus of the same isotope and that this might give useful information about level widths. Such a process would correspond to *resonance fluorescence* in atomic physics, which is an easily observed and well-studied phenomenon. In the nuclear context however, the study of resonance fluorescence presents severe experimental difficulties. These arise because the photon emitted by an excited nucleus does not in fact take away the full transition energy. To conserve linear momentum the emitting nucleus must recoil with a small but finite kinetic energy. Thus, the photon momentum being E_γ/c, we have

$$\sqrt{(2M_R\,T_R)}=\frac{E_\gamma}{c},$$

and therefore the kinetic energy T_R of recoil of the nucleus, mass M_R, is given by

$$T_R=\frac{E_\gamma^2}{2M_R\,c^2}.$$

Therefore $E_0=E_\gamma+\dfrac{E_\gamma^2}{2M_R\,c^2}.$ 10.7

The same consideration arises in the absorption process. The absorbing nucleus must recoil to take up the linear momentum of the incident photon, and hence the whole photon energy is not available as excitation energy. For absorption

$$E_\gamma=E_0+\frac{E_\gamma^2}{2M_R\,c^2}.$$

Taking for illustration the case of A approximately 200, E_0 approximately 400 keV, we find

$$\frac{E_\gamma^2}{2M_R\,c^2}\simeq 0{\cdot}9\ \text{eV}.$$

This shift in energy which occurs both in the case of emission and absorption is seen to be much greater than even the greatest estimated natural width, that of E1, quoted above. However, the emitting or absorbing nucleus is incorporated in an atom which has thermal motion. The thermal velocity gives rise to a Doppler shift which broadens the line. The full Doppler width is given by

$$2\Delta=2E_\gamma\sqrt{\left[\frac{2kT}{M_R\,c^2}\right]}.$$

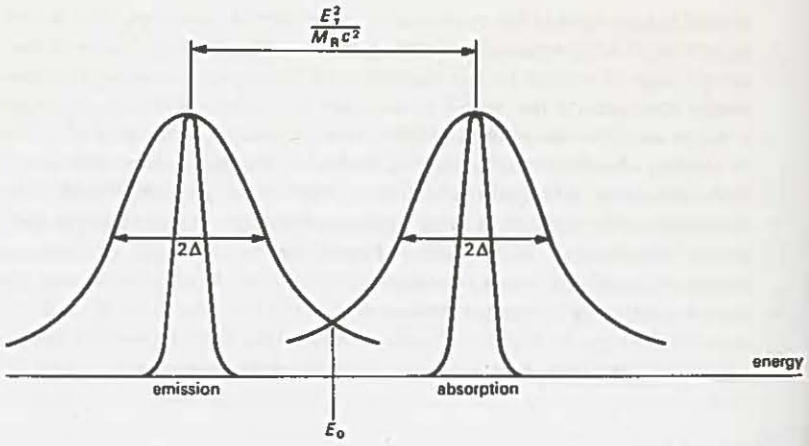

Figure 76 Shift of emission and absorption lines due to recoil of nucleus. The intrinsic width of the line (on a reduced vertical scale) is shown in the middle of the peaks, which are broadened by the Doppler shift arising from thermal atomic motion.

In our present illustration this means $2\Delta = 0{\cdot}4$ eV. The relationship of the emission to the absorption energy spectrum is shown in Figure 76. It is clear that the overlap, which will determine the extent to which resonance fluorescence takes place, is extremely small.

There are several possible methods for restoring the recoil energy and increasing the overlap. For example, if the source is moved relative to the absorber with velocity v, the emitted photon energy will be Doppler shifted by an amount $(v/c)E_\gamma$. If we calculate the velocity necessary to bring the emission and absorption spectra in Figure 76 into coincidence we find $v = 5{\cdot}1 \times 10^2$ m s^{-1}. Moon (1951) succeeded in achieving speeds of this magnitude by attaching a source to the tip of a high-speed rotor and demonstrated resonance fluorescence for 418 keV photons emitted by ^{198}Hg.

A second possibility for restoring the recoil energy arises when the photon is emitted so soon after a β- or γ-emission that the nucleus is still recoiling from the effect of the previous emission. For the values of A and E_0 considered above, the nucleus could have sufficient recoil momentum following the emission of a γ-ray of at least 400 keV or a β-particle of energy in excess of 140 keV. However, even when a source with a suitably fast transition can be found, the fact that the β-energy spectrum is continuous and also the requirement that the recoil has to be travelling at the correct angle with respect to the photon direction very severely limits the number of recoils which would contribute to fluorescent absorption.

The possibilities of experimentally studying nuclear resonance fluorescence were however completely altered by the discovery in 1958 by Mossbauer of

'recoilless' emission of γ-rays. This effect, now known as the *Mossbauer effect*, relies on the emitting and absorbing nuclei being incorporated in a crystal lattice. On the view that the lattice constitutes the quantum system, there is a certain minimum energy, namely that of one quantum, by which the lattice internal energy may be increased. If the kinetic energy of recoil of the nucleus following γ-emission is less than this minimum then there is no relative motion of the nucleus with respect to its neighbours possible and the whole lattice must recoil. On substitution of the lattice mass for the nuclear mass in equation 10.7 we see that the difference between E_γ and E_0 is now immeasurably small. The same consideration holds for absorption. We thus can have, with the source and the absorber in a suitable physical form, a complete overlap of the emission and absorption curves of Figure 76. When this coincidence has been achieved, a direct measure of the widths of these resonant curves becomes possible by introducing a relative motion between source and absorber. This motion leads to a Doppler shift and consequent separation of the emission and absorption curves. *The result of such an experiment is shown in Figure 77. It is seen that in the case of the 129 keV line of ^{191}Ir a velocity of 100 m s^{-1}, which corresponds to a Doppler shift of approximately 50×10^{-6} eV, is sufficient to make the overlap of the emission and absorption curves negligibly small. This transition in ^{191}Ir, which was that used by Mossbauer in establishing the effect, has been shown by a delayed coincidence experiment to have a half-life of $1{\cdot}3 \times 10^{-10}$ s. It is seen that the*

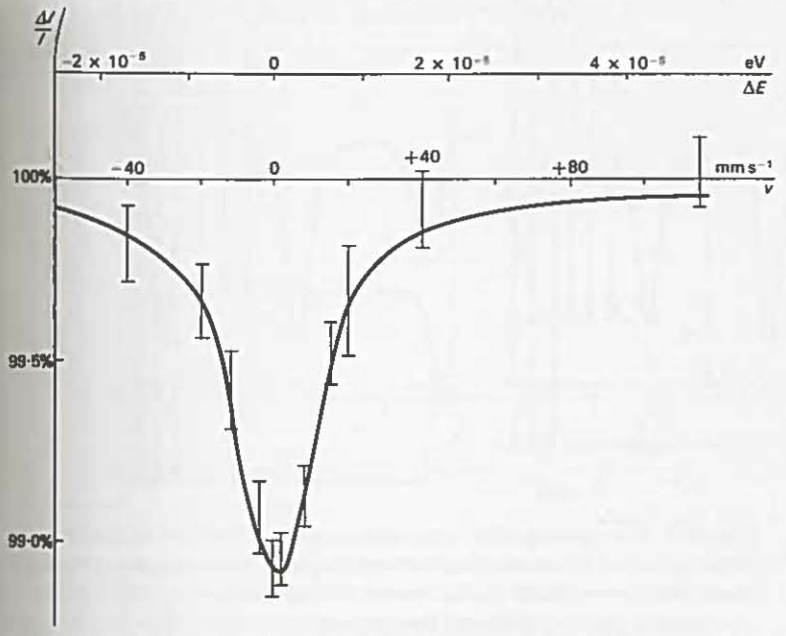

Figure 77 The results of the original Mossbauer experiment. The transmission of 129 keV γ-radiation from ^{191}Ir through an iridium absorber is measured as a function of relative velocity v of source and absorber

estimate of a width of about 5×10^{-6} eV which one would make using the uncertainty principle is in agreement with the measured transmission through the sample in Figure 77. The experimental curve which arises from moving an emission line of width Γ over an absorption line of the same width should have Lorentzian shape and line width 2Γ.

The special conditions which have to be satisfied by a transition for the Mossbauer effect to occur (namely that the transition energy should be small, so

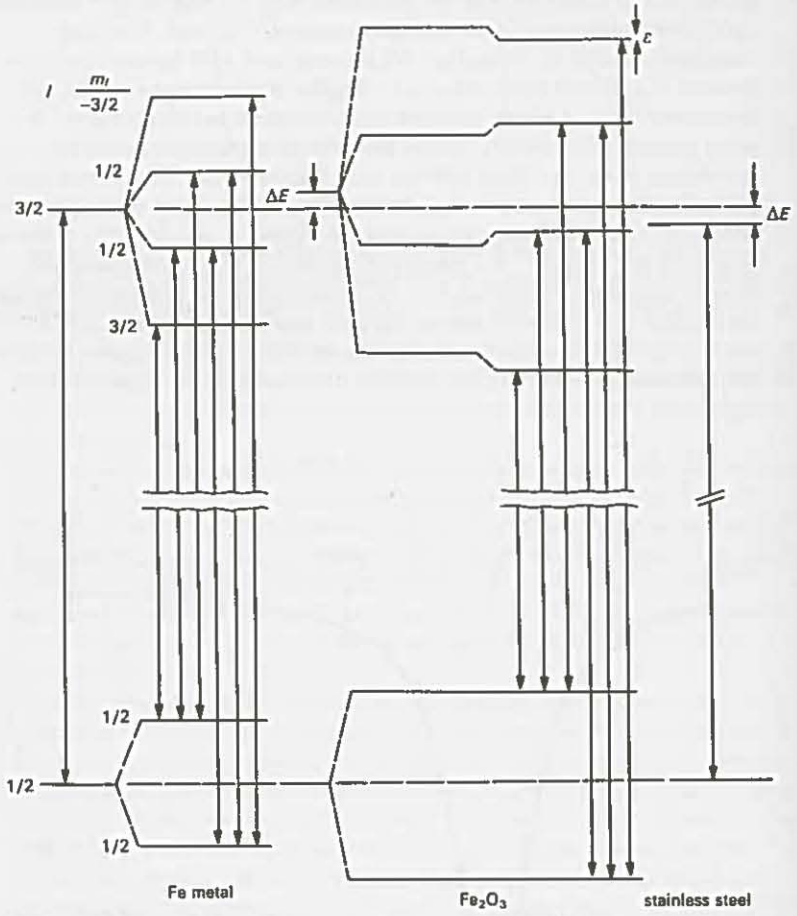

Figure 78 The splitting of the ground state and the 14·4 keV excited state in ^{57}Fe. In Fe metal there is a large internal magnetic field with which the nuclear dipole moment interacts, but because of the cubic symmetry of the lattice there is no electric field and hence no electric quadrupole interaction. In Fe_2O_3 there is an electric field gradient whose interaction with the electric quadrupole moment of the nucleus affects the magnetic substate of the upper level. In stainless steel the time-averaged magnetic field is zero and there is no electric field gradient. ΔE represents small shifts due to chemical binding effects

that the recoiling nucleus is locked in the lattice, and that the level width should be such that the Doppler-shift relative velocities are of a practical magnitude) will mean that the method will always be limited to very few transitions. About sixty suitable transitions have been found to date. In each case the level widths are as would be predicted for the measured half-lives.

While the Mossbauer effect has not added significantly to what was already known via the lifetime measurements, it has made possible hyperfine-structure measurements of very great sensitivity which lead to accurate determinations of nuclear moments. In this connection the nuclide ^{57}Fe has received much attention. The 14·4 keV magnetic dipole transition in ^{57}Fe has a half-life of $1{\cdot}4 \times 10^{-7}$ s and a width of $4{\cdot}6 \times 10^{-9}$ eV. In this case, the relative velocity of source and detector as small as 1 mm s^{-1} produces a Doppler shift large enough to affect the fluorescent absorption. When the Fe nucleus is embedded in stainless steel, the time-averaged magnetic field at the nucleus is zero. The levels are therefore not split and the emitted radiation is strictly monochromatic. When now an absorber of Fe metal is used, the large internal magnetic field splits the levels as shown in Figure 78. The metallic crystal lattice is such that there is no electric field at the Fe nucleus. In Fe_2O_3, however, there is an expected electric field gradient which causes shifts in the magnetic substates large enough to measure by the Mossbauer technique. The measured absorption curve in Figure 79 shows the accuracy with which the level spacings may be measured and values of μ and Q determined, as discussed in Chapter 8.

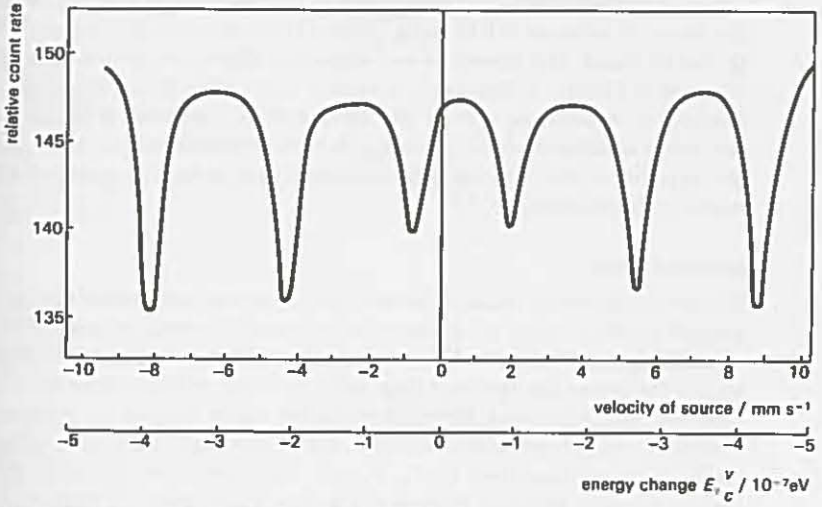

Figure 79 Absorption in Fe_2O_3 of the 14·4 keV γ-rays emitted in the decay of ^{57}Fe* formed by the decay of ^{57}Co incorporated in a stainless steel source. The six dips correspond to the six transitions of Figure 78

10.14 Transition strengths

The probability or strength of a transition, we have now seen, can be expressed in terms of a decay constant λ, a width Γ or a mean life τ. It is very often, however, convenient to take the single-particle predictions of section 10.6 as standards. When the observed width of a transition is divided by the appropriate single-particle width the ratio is said to give the transition strength in Weisskopf units.

When the measured transition strengths are examined it is found that, except for E2 transitions, the strengths in Weisskopf units are less than unity. In the case of E1 transitions and light nuclei the strengths may be as small as a few per cent. For E2 transitions, on the other hand, both in light and heavy nuclei there are many examples of strengths from ten to a hundred times the single-particle value.

An explanation of the enhancement of E2 transitions is to be sought in terms of the collective model of section 9.3. When this model is used instead of the single-particle model to calculate the transition matrix elements it is found that

$$B(\mathrm{E2}) = \frac{15}{32\pi} e^2 Q_0^2 \frac{(I+1)(I+2)}{(2I+3)(2I+5)}, \qquad 10.8$$

for a transition from a state spin $I+2$ to a state spin I. In this formula Q_0 is the static quadrupole moment. A large transition strength is therefore evidence of the existence of a large quadrupole moment.

The same reduced transition probabilities are involved in the cross-section for Coulomb excitation and the enhancement of E2 transitions is again found. From the measured values of B(E2), using formula 10.8, the static quadrupole moment Q_0 can be found. This provides a very important alternative method to that discussed in Chapter 8. Whereas in the earlier method the interaction of the quadrupole moment was with an internal electric field gradient, in the method now under consideration the interaction is with the radiation field. More reliance can be placed on the radiation-field calculation than on the calculation of internal electric field gradients.

10.15 Unbound states

We have, in discussing radiation widths, been concerned with bound states; the possible modes of decay we therefore had to consider were gamma emission, internal conversion and internal pair production. The total width of the bound level is the sum of the widths of these three processes, whose relative contributions have been discussed above. When the excitation energy exceeds the nucleon separation energy, and nucleon emission becomes possible, then the total width contains contributions from Γ_n, Γ_p, Γ_α, etc., the widths to be associated with particle emission. Since the lifetime of the state against decay by particle emission will be of the order of v/R, v being the particle velocity in the nucleus, R the nuclear radius, we find the mean life τ for this mode of decay to be about 10^{-21} s and the level width therefore to be hundreds of thousands of electronvolts. Thus the total width is dominated by the particle width, the gamma width making a negligible contribution.

10.16 Isobaric spin

The assumption that the specifically nuclear force between two nucleons is the same for nn, pp, np pairs results in important simplifications in nuclear theory. This hypothesis is referred to as the *charge independence* of nuclear force. If this is a valid hypothesis, it is to be expected that there will be similarities in the level structure of assemblies of a given number of nucleons, since the exchange of a proton for a neutron or vice versa should not affect the binding energy. We find in fact similarity in the level structure of mirror nuclei such as ^{7}Li and ^{7}Be. This can be seen in Figure 80. If we allow for the difference in Coulomb energy and the difference between neutron and proton rest masses, neither of which effects arises from nuclear forces, then the agreement in level position on an absolute scale is even better.

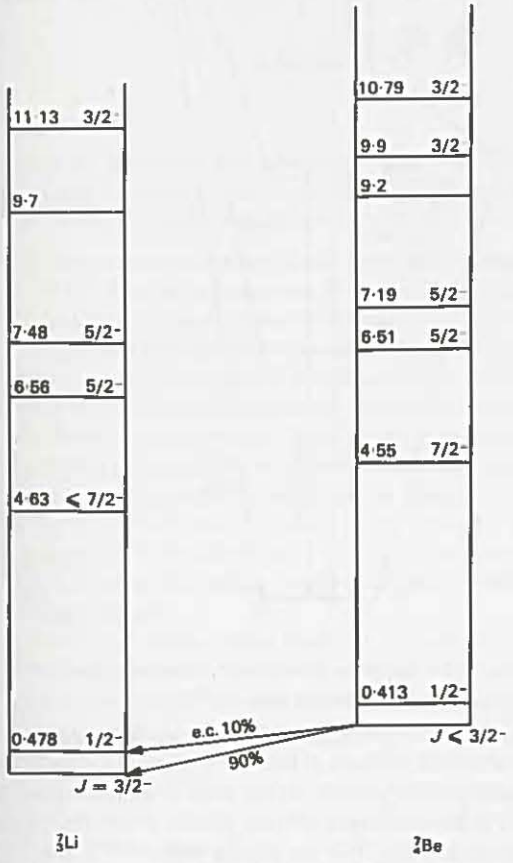

Figure 80 Energy level diagrams of ^{7}Li and ^{7}Be showing similarities in structure

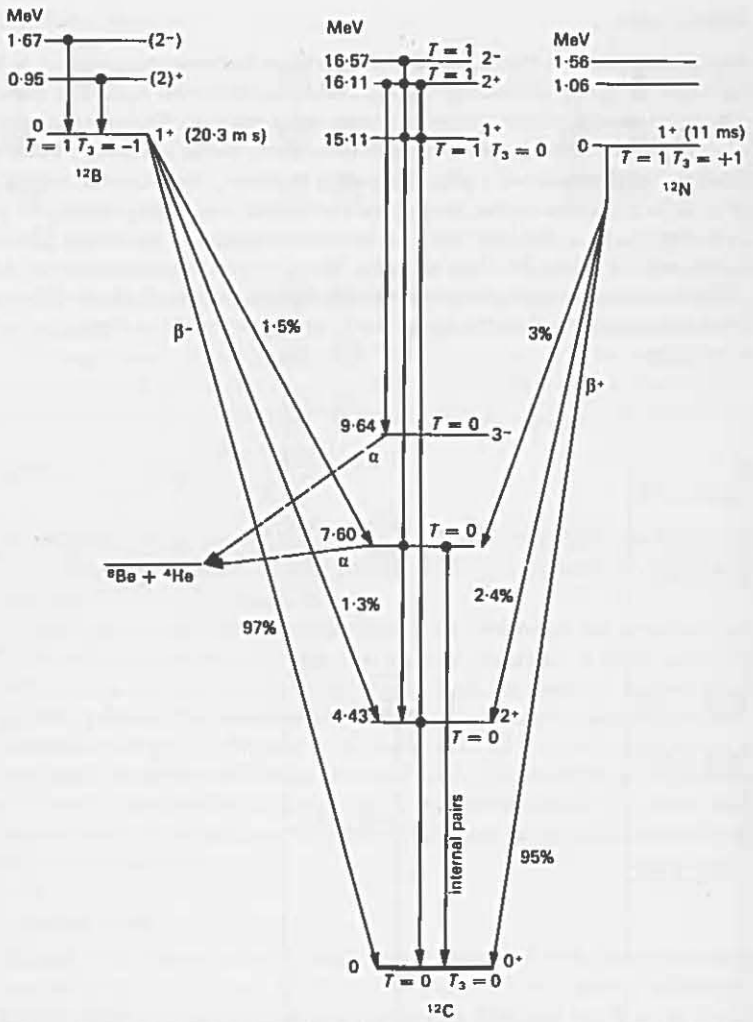

Figure 81 Isobaric triad with $A = 12$. Note the correspondence of the $T = 1$ states and the additional $T = 0$ states occurring only in ^{12}C

When we consider even-A nuclei in this connection, taking for example the isobars with $A = 12$ whose levels are shown in Figure 81, we find a state in the central nucleus corresponding to the ground state of both neighbouring isobars. This state is said to be the *isobaric analogue* of these ground states. Having regard to the Pauli exclusion principle, we see that the ground states of ^{12}B and ^{12}N must have the nucleons in spatial states with spins oriented as shown schematically in Figure 82. The analogue state of ^{12}C is shown for comparison. It is clear however

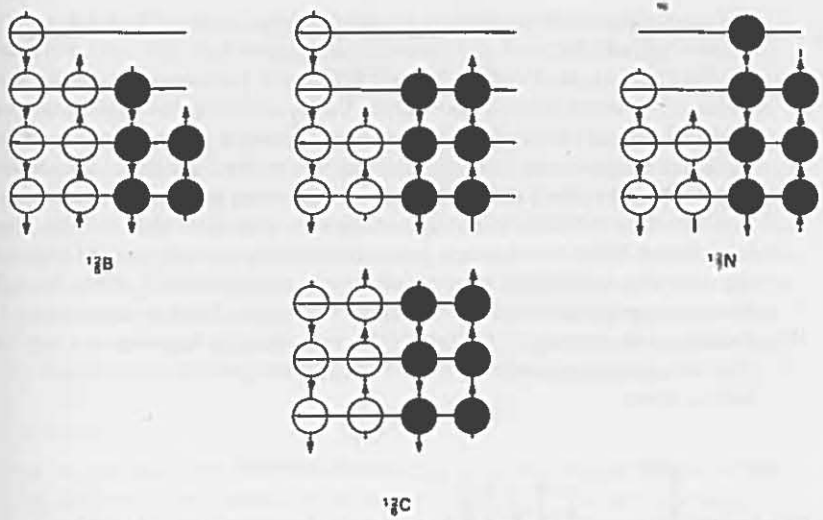

Figure 82 Schematic representation of $T = 1$ states in three members of an isobaric triad and $T = 0$ state in one member only. The Pauli exclusion principle dictates the number and spin orientation of the particles which may occupy each level

that a more symmetrical and hence more tightly bound arrangement is possible in ^{12}C but that this arrangement is not available to the other isobars because of the operation of the exclusion principle.

An elegant description of this situation can be given in terms of *isospin* (or *isobaric spin*), a concept first introduced by Heisenberg (1932) when it was misleadingly referred to as isotopic spin. Neutrons and protons are treated as two states of a nucleon, the charge of the proton and the mass difference between the proton and the neutron, believed to be electromagnetic in origin, being ignored. A new quantum vector T, the isospin, is introduced and given the property, similar to that of ordinary spin, of having allowed values $+\frac{1}{2}$ and $-\frac{1}{2}$ for its components T_3, along a specified direction. $T_3 = +\frac{1}{2}$ we associate with a proton and $T_3 = -\frac{1}{2}$ with a neutron (this, the currently accepted convention, is the opposite to that originally chosen).

Let us now take a pair of nucleons; the isospin of the pair is given by $T = 1$ or $T = 0$ from the addition of the two isospin vectors, carried out according to the rules applied to ordinary spin. There are then three possible components T_3 to be associated with $T = 1$ namely $T_3 = +1, 0, -1$. To $T_3 = +1$ will correspond two protons with antiparallel spin, to $T_3 = 0$ a neutron–proton pair, again with antiparallel spin and to $T_3 = -1$ a pair of neutrons with antiparallel spin. $T = 0$ will be a singlet, having only the possibility of $T_3 = 0$, which will correspond to a neutron–proton pair with parallel spin. On this interpretation the ground state of the deuteron with ordinary spin 1 has thus $T_3 = 0, T = 0$.

In the general case each proton in a nucleus will introduce $T_3 = +\frac{1}{2}$, each neutron will add $T_3 = -\frac{1}{2}$ and hence for the nucleus $T_3 = \frac{1}{2}(Z - N)$. For example, for ^{12}B $T_3 = -1$, for ^{12}C $T_3 = 0$, for ^{12}N $T_3 = +1$. It is now seen that the low-lying states in ^{12}C which have no analogues in the isobars are states with $T = 0$. The analogue state at 15·1 MeV in ^{12}C is the lowest-lying $T = 1$ state in that nucleus. At higher energies in all three isobars there will be $T = 2$ states, the lowest-lying of which will be expected to be analogues of the ground state of ^{12}Be and ^{12}0.

The isospin substates will be degenerate only in so far as the Coulomb interaction is neglected. When the Coulomb interaction is taken into account the level splits in the same way as magnetic substates separate in a magnetic field. When the splitting becomes appreciable, as would be expected in nuclei of high atomic number, then T ceases to be meaningful. In view of this expectation it has come as a surprise that isobaric analogue states can still be recognized in nuclei with A-values as high as ninety.

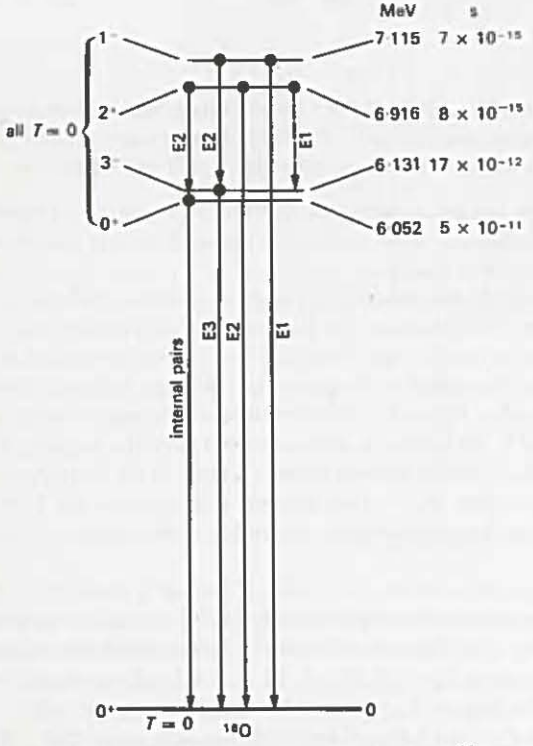

Figure 83 Transitions between some levels of ^{16}0 to illustrate the operation of the isobaric spin selection rule in electric dipole transitions. The E1 transition from the 6·916 MeV level to the 6·052 level is not observed and the E1 transition from the 7·115 MeV level to the ground state has a half-life several orders of magnitude longer than the Weisskopf estimate, as can be seen from Figure 69

It is found that, in radiative transitions, alongside the selection rules of section 10.5.3 we have to place isospin selection rules. In a radiative transition in which only one nucleon changes its state $\Delta T = 0$ or ± 1. This does not lead to any immediately practical result as $T = 2$ states lie very high in the level diagrams of light nuclei. However, for electric dipole transitions in self-conjugate nuclei (i.e. having $Z = N$) there is the special rule that $\Delta T = \pm 1$. This is of practical importance as very many low-lying states have $T = 0$, and $T = 0 \rightarrow T = 0$ is forbidden by this rule. This forbiddenness arises because in both initial and final states the neutrons and protons are occupying identical nucleon states. There is thus in the transition no separation of neutron and proton distributions, which is necessary for there to be an induced dipole moment. The operation of this isobaric spin selection rule can be seen in Figure 83 in the case of ^{16}O. It is seen that the rule is not inviolable but that if it is not obeyed the transitions are considerably inhibited.

10.17 Summary

We have seen that the broad picture now held of nuclear excited states is of low-lying collective states, vibrational in nature in the case of the spherical nuclei, rotational in the case of the deformed nuclei, with single-particle states lying above. Still higher lie states corresponding to excitations of the nuclear core as distinct from collective effects in the outer shell. These higher states are involved in photonuclear reactions, and, lying above the particle separation energy, they are capable of decaying by particle emission.

In light nuclei similarities are found in the level structures of isobars which encourages the introduction of a further quantum number, isobaric spin, to join spin and parity in the designation of a nuclear level.

Chapter 11
Nuclear Fission

11.1 Introduction

In section 5.11 a brief and formal discussion was given of the process of fission, in which a heavy nucleus breaks into two main fragments with the release of an amount of energy which even by nuclear standards is spectacular. In sufficiently heavy nuclei fission takes place spontaneously from the ground state, competing as a decay process with α-decay. A theoretical treatment can be given in terms of the concepts introduced in α-decay theory. Fission may also be induced by bombarding a heavy element with neutrons or other nuclear projectiles, or by exposing the element to a beam of high-energy X-rays. *Induced fission* is a special case of a nuclear reaction, in which a compound nucleus is formed in an excited state and fission is one of the several possible modes of decay. All of these decay modes, including fission, will have widths as defined in section 10.7. A discussion of induced fission more properly finds its place in the companion volume, W. M. Gibson *Nuclear Reactions*, Penguin, 1971. In the present chapter we are concerned with fission as a nuclear decay process.

11.2 Experimental aspects of fission

Experimentally, fission is observed to involve the emission of two massive fragments, each having kinetic energy of about 75 MeV. In the case of spontaneous fission the fragments are not usually of equal mass; the fission is then said to be *asymmetric*. In the case of induced fission the asymmetry in mass decreases with increase in bombarding energy and the fission may become *symmetric*. In Figure 84 are plotted the mass distributions of fission fragments for the isotopes ^{234}U, ^{236}U and ^{240}Pu, the compound nuclei formed by neutron capture into ^{233}U, ^{235}U and ^{239}Pu. Note that the ratio of the yields at the asymmetric peaks to the symmetric yield is so large that a logarithmic scale has been used in the presentation.

All of the nucleons of the original nucleus are not usually accounted for by the composition of the two fragments. Because of the increase in neutron excess with mass number of stable nuclei, there are more neutrons available than the fission fragments can stably contain. As a consequence, not only are the fission fragments created with Z- and N-numbers lying well off the stability area on the nuclear chart, by virtue of excess neutrons, but in addition free neutrons are released 'promptly' in the process. The energy spectrum of these neutrons peaks at 1 MeV and falls off exponentially, the 'tail' extending to about 15 MeV. The emission of

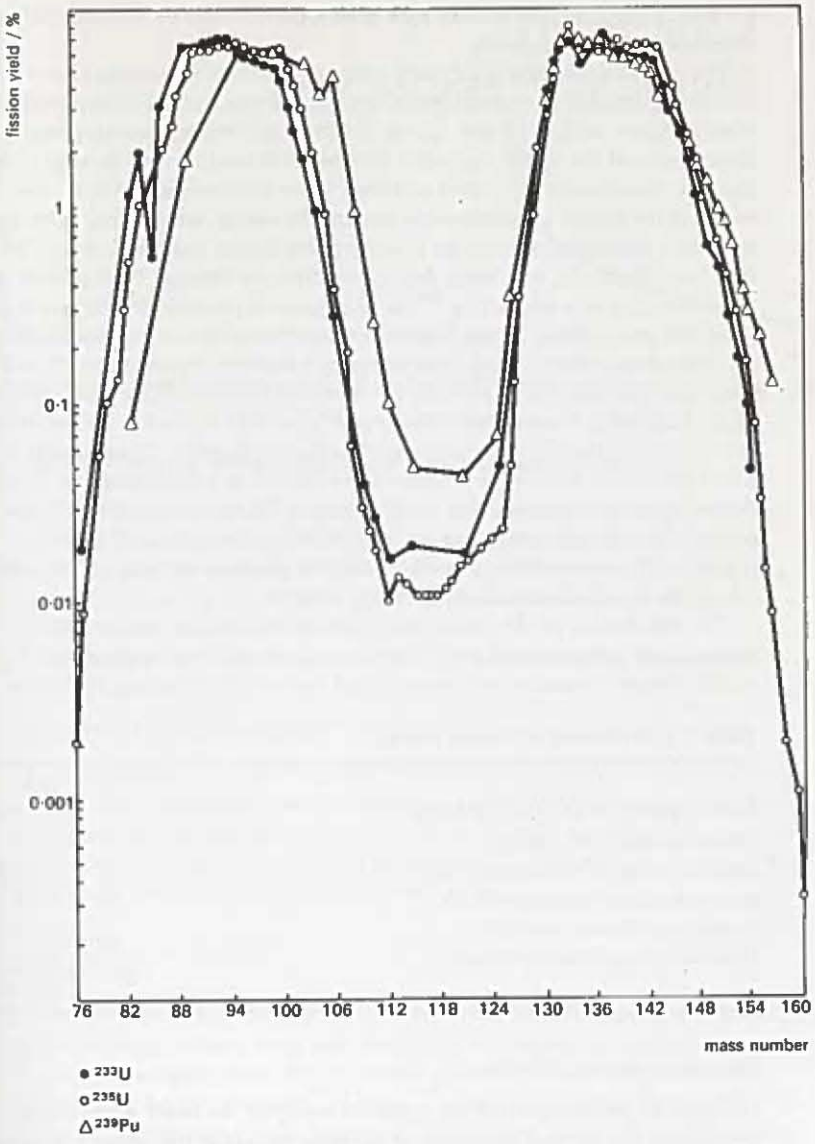

Figure 84 The mass distribution of fission fragments in the slow-neutron fission of ^{233}U, ^{235}U and ^{239}Pu

prompt neutrons as products of the fission events and their potentiality for inducing further fission events make a chain reaction a practical possibility.

When only two charged fragments are emitted the fission is termed *binary*. In a relatively small percentage of the fission decays, usually about a few tenths of one

per cent, a third charged particle such as an α-particle may be emitted; the process is then termed *ternary fission.*

The emission of γ-rays is a further accompaniment of the fission process. This is to be expected as a consequence of the rapid charge rearrangement which takes place as fission occurs. To sum up, we note that the *primary* process consists of the emission of the fission fragments together with neutrons and prompt γ-rays and very occasionally other light particles. There are *secondary* effects, also involving the release of considerable amounts of energy, which occur later. An important secondary effect is the β-decay of the fission fragments. As can be seen from Figure 84, very many β-active nuclides are formed. The half-lives range from a fraction of a second (e.g. ^{85}As: 0·43 seconds) to millions of years (e.g. ^{129}I: $1{\cdot}6 \times 10^7$ years). Many of the fragments when formed are so far from stability that several successive decays, each involving a neutron-to-proton switch, and hence the emission of a β^- particle, are necessary before stability is achieved. The nuclei involved in these decay chains may of course be formed in excited states and γ-rays may therefore be involved in the decay processes. Consequently it is found that β-rays and γ-rays continue to be emitted at a decreasing rate from fission fragments removed from fissile materials. We noted in section 6.1 that neutrons are emitted from some nuclides following the β-decay of fission fragments. These constitute secondary *delayed* neutrons and play an important role in the control mechanisms of nuclear reactors.

The distribution of the fission energy among the primary and secondary particles and radiation is of great importance in the practical application of nuclear fission in reactors and weapons and is given for interest in Table 7.

Table 7 Distribution of Fission Energy

	MeV
Kinetic energy of fission fragments	165 ± 5
Instantaneous γ-ray energy	7 ± 1
Kinetic energy of fission neutrons	5 ± 0·5
β-particles from fission products	7 ± 1
γ-rays from fission products	6 ± 1
Neutrinos from fission products	10
	200 ± 6

11.3 Elementary theory of fission

In Figure 85 we have plotted the potential energy of the heavy nucleus as a function of the distance of separation between centres of the fission fragments, here regarded as being of spherical shape with radii R_1 and R_2. From very large separation distances down to a distance $R_1 + R_2$, assuming the spheres to remain undistorted until they touch, this curve is a hyperbola since

$$V = \frac{e^2 Z_1 Z_2}{r}.$$

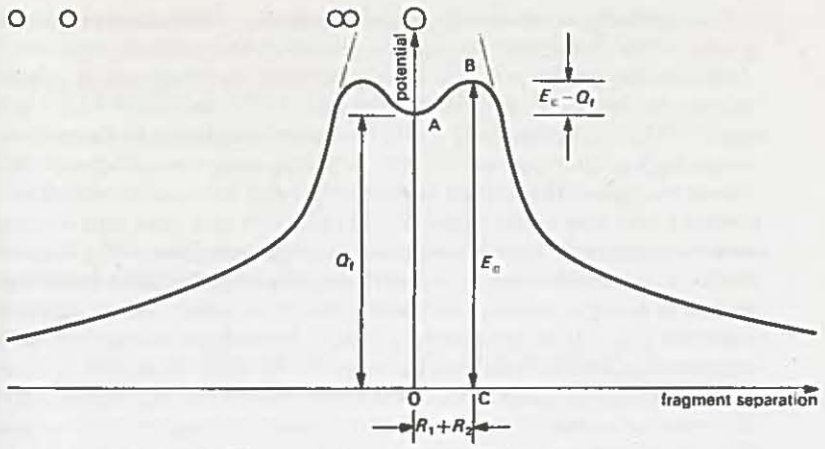

Figure 85 Potential energy against fission fragment separation

From the separation at which the fragments touch down to zero separation, where they have completely merged to form one nucleus, there is no simple way of finding the form of this potential curve. We do know however that it must pass through A where OA = Q_f is given by the difference between the nuclear mass and the sum of the masses of the fragments.

To establish the relative lengths of OA = Q_f and CB = E_c let us consider the particular case of

$$^{236}_{92}U^{144} \rightarrow {}^{95}_{36}Kr^{59} + {}^{141}_{56}Ba^{85}.$$

The excess masses of ^{236}U, ^{95}Kr and ^{141}Ba being 42·52 MeV, − 58·34 MeV and − 79·97 MeV respectively, we find that Q_f = 180·83 MeV. If we take the nuclear unit radius R_0 (see section 3.14) to be 1·48 fm, in order to evaluate $R_1 + R_2$, and extrapolate the hyperbola, as shown in Figure 85, to the point of contact of the spheres, the maximum of the curve is found to be

$$\frac{e^2 Z_1 Z_2}{R_0(A_1^{\frac{1}{3}} + A_2^{\frac{1}{3}})} = 201 \text{ MeV}.$$

It is however to be expected that the deformation of the fragments and the details of the fall off of nuclear force will remove the sharpness and round the curve off to a lower maximum value. We can invoke a very important difference in the behaviour of the two isotopes ^{235}U and ^{238}U to establish the difference $E_c - Q_f$. When natural uranium (99·27 per cent ^{238}U; 0·72 per cent ^{235}U) is bombarded with slow neutrons, fission is induced in the ^{235}U isotope only; when, however, the neutron energy is increased to 1·2 MeV, fission is induced in ^{238}U. We interpret this as establishing that there is a threshold energy for the process

$$^{238}\text{U} + \text{n} \rightarrow {}^{239}\text{U}^* \rightarrow \text{X} + \text{Y},$$

and that there is no corresponding threshold when the lighter isotope captures a neutron. If we now, from the mass values, calculate the extent to which the compound nuclei ^{236}U and ^{239}U are excited following the capture of a slow neutron, we find that it is 6·5 MeV in the case of ^{236}U and only 4·8 MeV in the case of ^{239}U. This difference in excitation energy is explained by the neutron completing a neutron pair in ^{236}U and the pairing energy becoming available for internal excitation. The neutron added to ^{238}U does not have the possibility of forming a pair. Now Q_f in the case of ^{239}U is 181·14 MeV, very little different from the value for ^{236}U. The energy curve at large separations of the fragments should be the same for both isotopes. The existence of a threshold in the case of the heavier isotope, and its absence in the case of the lighter, is then satisfactorily explained if $E_c - Q_f$ is approximately 6 MeV. The addition of a neutron to the lighter isotope then provides enough energy for the fission fragments to 'go over the potential barrier'. In the case of the heavier isotope the addition of a neutron still leaves the excitation energy such that a barrier is presented to the outgoing fission fragments.

The threshold for induced fission mentioned above is only an apparent threshold. Barrier penetration, while unlikely, still has a finite probability, so that the onset of fission will not be expected to commence abruptly at a well-defined energy but to increase continuously with increasing excitation energy as the width of the barrier to be penetrated decreases.

In the case of nuclei lighter than uranium, $E_c - Q_f$ will be greater and fission will be more difficult to induce. With heavier nuclei on the other hand, $E_c - Q_f$ will be expected to decrease; when it attains small values spontaneous fission by barrier penetration will become more likely, the half-life for the process getting progressively shorter as $E_c - Q_f$ diminishes.

A deeper understanding of the phenomenon of fission requires a study of nuclear behaviour in the neighbourhood of the potential-energy maximum. This can only be undertaken in terms of a specific nuclear model. N. Bohr and Wheeler (1939) laid the foundations for tackling the problem in terms of the liquid-drop model. The nucleus in its ground state was likened to a spherical drop of incompressible liquid of uniform density and uniformly distributed charge. When deformed from its spherical shape, its potential energy was assumed to be determined by the surface- and Coulomb-energy terms defined in section 5.5. We now proceed firstly to investigate in terms of these assumptions the effect of a small deformation in order to explore the stability of the spherical shape, and secondly to consider the effect of deformations large enough to take the system through the potential-energy maximum.

11.4 Nuclear stability: small deformations

The stability of the electrically charged drop against small disturbances will be determined by the size of the increase in surface energy, compared to the decrease in Coulomb energy, caused by the departure from spherical shape. These energy changes can be calculated in purely classical terms. Assume the small deformation to be from a spherical shape, radius R, to the shape of a spheroid with equal

semi-axes b and the third semi-axis equal to c. The incompressibility of the liquid demands constancy of volume; hence we have

$$\tfrac{4}{3}\pi R^3 = \tfrac{4}{3}\pi c b^2.$$

We now introduce ϵ', writing

$$c = R(1+\epsilon'), \qquad b = \frac{R}{(1+\epsilon')^{\frac{1}{2}}},$$

where ϵ' is a small quantity. On deformation, the surface energy, due to the increase in surface area, is increased from

$$a_s A^{\frac{2}{3}},$$

the value we attributed in section 5.5 to the spherical nucleus, to

$$a_s A^{\frac{2}{3}}(1 + \tfrac{2}{5}\epsilon'^2),$$

higher powers of ϵ' being neglected. The Coulomb energy, on the other hand, is reduced from the spherical value of

$$a_C \frac{Z^2}{A^{\frac{1}{3}}}$$

to $$a_C \frac{Z^2}{A^{\frac{1}{3}}}\left[1 - \frac{1}{5}\epsilon'^2\right],$$

to the same order of accuracy. We therefore conclude that, for the particular form of deformation here being considered, the drop will be stable or unstable when slightly disturbed depending on whether $\frac{2}{5}a_s A^{\frac{2}{3}}$ is greater or less than $\frac{1}{5}a_C Z^2/A^{\frac{1}{3}}$, i.e. whether Z^2/A is less or greater than $2a_s/a_C$. This critical value we denote by

$$\left[\frac{Z^2}{A}\right]_c.$$

For the values of a_s and a_C introduced in section 5.5 it is approximately equal to 44. We recollect that mass-energy considerations alone in section 5.11 lead to the conclusion that symmetric spontaneous fission 'over the barrier' became possible for

$$\frac{Z^2}{A} \gtrsim 50.$$

Asymmetric fission may be possible for lower values of this quantity. Also, allowing for the probability for barrier penetration, we will not expect a sudden onset of spontaneous fission at a particular value of Z^2/A. However, it is very convenient to form the ratio of Z^2/A to $(Z^2/A)_c$ for any particular nucleus and to regard this ratio as a measure of the stability of the nucleus against spontaneous fission. It is usually denoted by x and called the *fissionability parameter*. In Figure 86 are plotted some measured values of spontaneous-fission half-lives against Z^2/A to show the essential validity of these concepts.